HHS Public Access

Author manuscript

Curr Biol. Author manuscript; available in PMC 2022 September 13.

Published in final edited form as:

Curr Biol. 2021 September 13; 31(17): 3810–3819.e4. doi:10.1016/j.cub.2021.06.052.

Ankyrin-dependent Na^+ channel clustering prevents neuromuscular synapse fatigue

Chuansheng Zhang[1], **Abhijeet Joshi**[1], **Yanhong Liu**[1], **Ozlem Sert**[1], **Seth Haddix**[1], **Lindsay H. Teliska**[1], **Anne Rasband**[1], **George G. Rodney**[2], **Matthew N. Rasband**[1]

[1]Department of Neuroscience, Baylor College of Medicine, Houston, TX, 77030, USA.

[2]Department of Physiology, Baylor College of Medicine, Houston, TX, 77030, USA.

SUMMARY

Skeletal muscle contraction depends on activation of clustered acetylcholine receptors (AchRs) and muscle-specific Na^+ channels (Nav1.4). Some Nav1.4 channels are highly enriched at the neuromuscular junction (NMJ) and their clustering is thought to be essential for effective muscle excitation. However, this has not been experimentally tested, and how NMJ Na^+ channels are clustered is unknown. Here, using muscle-specific AnkyrinR, AnkyrinB, and AnkyrinG single, double, and triple-conditional knockout mice we show that Nav1.4 channels fail to cluster only after deletion of all three ankyrins. Remarkably, ankyrin-deficient muscles have normal NMJ morphology, AchR clustering, sarcolemmal levels of Nav1.4, and muscle force, and they show no indication of degeneration. However, mice lacking clustered NMJ Na^+ channels have significantly reduced levels of motor activity and their NMJs rapidly fatigue after repeated nerve-dependent stimulation. Thus, the triple-redundancy of ankyrins facilitates NMJ Na^+ channel clustering to prevent neuromuscular synapse fatigue.

Graphical Abstract

Address correspondence to Lead Contact: Matthew N. Rasband, Department of Neuroscience, Baylor College of Medicine, One Baylor Plaza, Houston, Texas 77030, Tel: 713-798-4494, Fax: 713-798-3946, rasband@bcm.edu, Twitter: @MattRasband.

AUTHOR CONTRIBUTIONS

C.Z. designed and conducted experiments, analyzed results, and edited the manuscript. Y.L., A.J., O.S., S.H., L.T., A.R., and G.G.R. performed and analyzed results, and M.N.R. conceived and supervised the project, designed and analyzed experiments, and wrote the manuscript.

DECLARATION OF INTERESTS

The authors declare no competing interests.

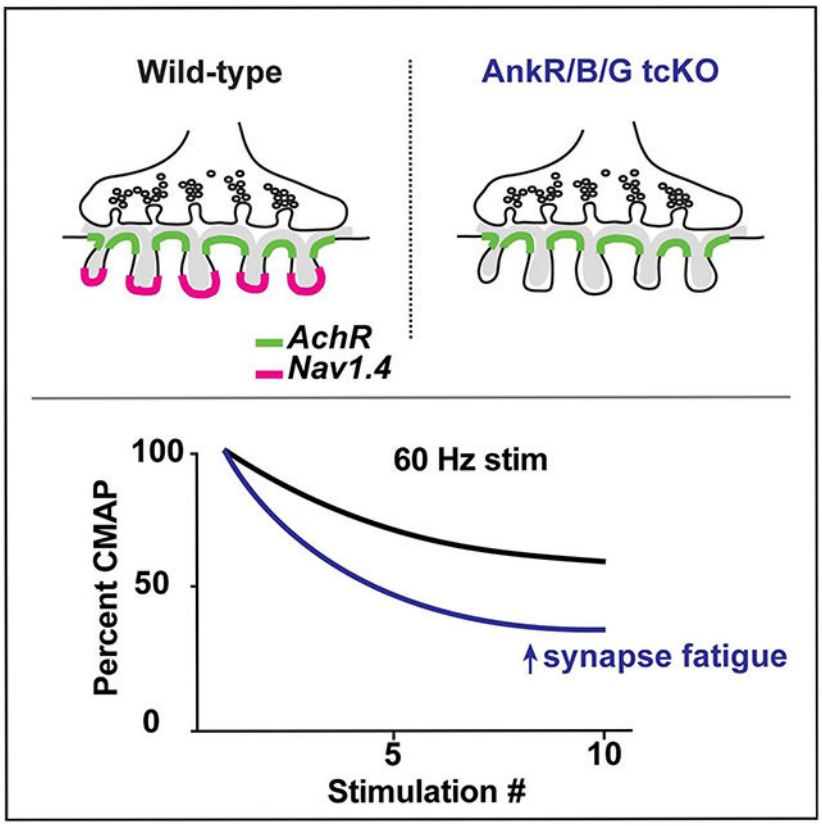

eTOC blurb:

Zhang et al. show that Nav1.4 Na^+ channels are clustered at the neuromuscular junction (NMJ) through ankyrin scaffolding proteins. Their experiments uncouple the function of non-synaptic Nav1.4 from its role at the NMJ. Neuromuscular junctions without clustered Nav1.4 fatigue more easily.

Keywords

neuromuscular junction; scaffold; ion channel

INTRODUCTION

The neuromuscular junction (NMJ) has been successfully used as a model for synapse development, function, and refinement. These studies revealed in remarkable detail neuron-derived factors and activity-dependent mechanisms responsible for muscle membrane specialization and postsynaptic neurotransmitter receptor clustering [1]. However, AchRs are not the only ion channel necessary for muscle contraction. AchR activation generates an endplate potential that activates the muscle-specific Nav1.4 Na^+ channels required for the muscle action potential [2]. Although Nav1.4 channels are found throughout the sarcolemma, they are also highly and specifically clustered in the junctional folds of the endplate [3]. NMJ Na^+ channels are proposed to be important for effective muscle excitation

by amplifying the effect of transmitter action on AchRs [4]. Furthermore, computational modeling suggests that structural variation in synapses may be compensated for by the high density of postsynaptic Nav1.4 [5]. However, the function of clustered NMJ Nav1.4 channels has not been directly tested since it has not been possible to separate the function of sarcolemmal Nav1.4 from NMJ Nav1.4.

In contrast to AchRs, NMJ Na^+ channel clustering mechanisms are unknown. Much is known about the molecular mechanisms responsible for Na^+ channel clustering at nodes of Ranvier in myelinated axons where action potentials are regenerated to facilitate rapid action potential conduction [6]. For example, in the peripheral nervous system two independent Schwann cell-directed mechanisms cluster nodal Na^+ channels. First, the secreted and Schwann cell-derived protein gliomedin clusters the axonal cell adhesion molecule Neurofascin 186 (NF186), which then recruits the Na^+ channel-binding and scaffolding protein AnkyrinG (AnkG); AnkG and Na^+ channels are then stabilized in the membrane and linked to the actin cytoskeleton by β4 spectrin. Second, paranodal axoglial junctions flanking each node assemble a β2 spectrin-dependent cytoskeleton that functions as a barrier to restrict AnkG and Na^+ channels to nodes. In the absence of AnkG or β4 spectrin, a cytoskeletal complex consisting of AnkyrinR (AnkR) and β1 spectrin can compensate to cluster and maintain nodal Na^+ channels, but in the absence of both AnkG and AnkR, Na^+ channels fail to cluster [7]. Like nodes of Ranvier, NMJs have clustered Na^+ channels, ankyrins, spectrins, and cell adhesion molecules. For example, both AnkG and AnkR have been reported to co-exist at the NMJ [8, 9], and to colocalize with Na^+ channels and a molecularly unidentified β spectrin [10]. Thus, nodes of Ranvier are an attractive paradigm for the mechanism of NMJ Na^+ channel clustering [11]. If the mechanisms responsible for Nav1.4 channel clustering were identified and subsequently blocked, it would then be possible to experimentally test the contribution of clustered Nav1.4 to neuromuscular synapse and muscle function.

To this end, we generated muscle-specific ankyrin-deficient mice. We found it was necessary to simultaneously remove all three vertebrate ankyrins to block NMJ Na^+ channel clustering. Using these mice, we directly tested the role of clustered NMJ Na^+ channels in neuromuscular synapse function. Unexpectedly, mice with ankyrin-deficient muscles were viable, had normal NMJ morphology and muscle strength, and showed no indication of muscle degeneration. Nevertheless, mice lacking clustered NMJ Na^+ channels were significantly less active and their neuromuscular synapses fatigued more quickly. Together, our results reveal an ankyrin-dependent mechanism for NMJ Na^+ channel clustering that increases the safety factor for action potential initiation by preventing neuromuscular synapse fatigue.

RESULTS

Nav1.4 Na^+ channels are clustered at α-Bungarotoxin (Btx)-labeled NMJs (Figures 1A, B). These channels can also be detected at NMJs using a pan Na^+ channel (PanNav) antibody (Figure 1C). Consistent with previous reports [3], we found that NMJ Nav1.4 channels accumulate postnatally and become highly enriched by 3 weeks after birth (Figure 1E); the increase in channel density is concomitant with an increase in NMJ area (Figure 1F).

All vertebrate Na^+ channels, including Nav1.4, have an ankyrin-binding motif located in the cytoplasmic linker between domains II and III; in neurons, this motif is necessary and sufficient for ankyrin-dependent targeting of channels to axon initial segments (AIS) and nodes of Ranvier [12, 13]. The NMJ is also highly enriched with AnkG (Figure 1D), suggesting that AnkG may cluster Nav1.4 at the NMJ. AnkG is a large scaffolding protein that undergoes extensive alternative splicing with major variants including 190, 270, and 480 kDa forms. Using antibodies that specifically recognize AnkG480, and consistent with previous reports [14], we found that AnkG480 is prominently located at nodes of Ranvier and weakly in the distal unmyelinated motor axon presynaptic terminal. However, AnkG480 is not present at the NMJ endplate (Figure 1G). Using antibodies that recognize AnkG epitopes common to both AnkG270 and AnkG480, we found very strong immunoreactivity at the NMJ (Figure 1H), indicating that AnkG270 is the variant present at the NMJ endplate. Like Na^+ channels, KCNQ2 K^+ channels are clustered at AIS and nodes of Ranvier [15], and they have an AnkG-binding motif very similar to the one found in Na^+ channels [16]. Immunostaining revealed that KCNQ2 K^+ channels are also found at the NMJ (Figure 1I).

The remarkable molecular similarities between AIS, nodes of Ranvier, and NMJ caused us to consider whether other nodal and AIS proteins, including β4 spectrin and the ankyrin-binding cell adhesion molecule NF186, which can be linked to the extracellular matrix, might also be part of the NMJ (Figure 1J). Immunostaining showed that although β4 spectrin and neurofascin (Nfasc) are highly enriched at nodes, they are not enriched at the NMJ (Figures 1K, L). At nodes of Ranvier, but not AIS, Na^+ channels may also be clustered by a complex of AnkR and β1 spectrin when AnkG or β4 spectrin is absent [7, 17]. Although we did not find β4 spectrin enriched at the NMJ, we did find both AnkR and β1 spectrin highly clustered at the NMJ (Figures 1M, N), confirming that AnkG and AnkR co-exist at the NMJ [8] and suggesting that they may be linked to the actin cytoskeleton through β1 spectrin. One previous report suggested that AnkB may also play important roles in NMJ function and assembly [18]. However, we only found presynaptic, axonal AnkB (Figure 1O). Together these results suggest that Nav1.4 Na^+ channels are clustered at the NMJ through the cytoskeletal scaffolding proteins AnkG and AnkR, and that this complex may be stabilized in the postsynaptic junctional folds by β1 spectrin.

Muscle-specific loss of single ankyrins

To determine the molecular mechanisms of NMJ Nav1.4 channel clustering we generated conditional knockout (cKO) mice lacking skeletal muscle AnkR, AnkB, or AnkG by crossing *Myo-Cre* mice with $Ank1^{f/f}$, $Ank2^{f/f}$, or $Ank3^{f/f}$ mice, respectively (hereafter referred to as AnkR cKO, AnkB cKO, or AnkG cKO). Immunoblots of muscle homogenates show a complete loss of AnkG270, and the nearly complete loss of AnkB and AnkR (Figure 2A); the residual AnkB and AnkR may reflect detection of axonal and red blood cell ankyrins, respectively. Immunostaining of NMJs in AnkG ckO mice show the complete loss of NMJ AnkG (Figure 2B), while Nav1.4, AnkR, and β1 spectrin were still highly enriched (Figures 2C-E). Similarly, AnkR cKO mice lacked AnkR at the NMJ (Figure 2G) but still had robustly clustered Nav1.4 (Figure 2H). AnkB cKO mice showed low levels of axonal AnkB (Figure 2J), but unperturbed NMJ Nav1.4 channel clustering (Figure 2K). In contrast to Nav1.4, we found that loss of AnkG was sufficient to block the clustering

of KCNQ2-containing K^+ channels (Figure 2F). Consistent with the sufficiency of AnkG, KCNQ2 was still clustered at the NMJ in AnkR and AnkB cKO mice (Figures 2I, L). When we measured the ratio of NMJ Nav1.4 immunofluorescence to Btx we found no difference between controls (*Ank1*$^{f/f}$, *Ank2*$^{f/f}$, or *Ank3*$^{f/f}$ mice) and AnkR cKO, AnkB cKO, or AnkG cKO mice (Figure 2J). Furthermore, all control and cKO mice performed normally on the rotarod (Figure 2K). Together, these results show that no single ankyrin is required for NMJ Nav1.4 channel clustering, but AnkG alone is required to cluster NMJ KCNQ2 subunit-containing K^+ channels.

Muscle-specific loss of two ankyrins simultaneously

To further define the redundancy among ankyrins for NMJ Nav1.4 channel clustering, we generated double-conditional knockout (dcKO) mice lacking skeletal muscle AnkB and AnkG (AnkB/G dcKO), AnkR and AnkG (AnkR/G dcKO), or AnkR and AnkB (AnkR/B dcKO). We compared NMJ Nav1.4 channel clustering in the dcKO mice to their floxed controls (Figures 3A-I). We confirmed loss of NMJ ankyrins (although presynaptic axonal AnkB was preserved; Figure 3B) in the AnkB/G and AnkR/B dcKO mice), but found that Nav1.4 clustering still occurred in all dcKO mice (Figures 3B, E, and H). Immunostaining for AnkR in AnkB/G dcKO mice and AnkG in AnkR/B dcKO mice showed that these scaffolds were highly enriched at the NMJ in the dcKO mice and are sufficient to cluster Nav1.4 (Figures 3C and 3I). However, we did not detect enrichment for AnkB at the postsynaptic NMJ in AnkR/G dcKO mice (Figure 3F). Instead, we only observed axonal AnkB despite the persistent clustering of NMJ Nav1.4. Nevertheless, measurement of the ratio of NMJ Nav1.4 to Btx showed that although Nav1.4 was present in all dcKO synapses, AnkB/G and AnkR/G dcKO mice had significantly reduced Nav1.4 channel density (Figure 3J). In contrast, AnkR/B dcKO mice had normal NMJ Nav1.4 channel density (Figures 3H, J). Despite the reduced NMJ Nav1.4 in AnkB/G and AnkR/G dcKO mice, they were indistinguishable from their floxed controls on the rotarod (Figure 3K). These results suggest that there is triple-redundancy for NMJ Nav1.4 channel clustering.

Muscle-specific loss of all ankyrins

To determine if ankyrins are required for NMJ Nav1.4 channel clustering and muscle function in general, we generated triple conditional knockout (tcKO) mice lacking AnkR, B, and G (AnkR/B/G tcKO). ImmunobIots of muscle homogenates showed loss of all ankyrins (Figure 4A). Importantly, morphometric analysis of AchR and endplate area, NMJ fragments, and compactness all showed no difference between triple floxed control mice and AnkR/B/G tcKO mice (Figures 4B-E), indicating that loss of ankyrins does not disrupt NMJ structure. In contrast to floxed controls (Figure 4F), and all cKO and dcKO mice (Figures 2 and 3), we found that AnkR/B/G tcKO mice lacked all NMJ clustering of Nav1.4 (Figure 4G). The ratio of Nav1.4 to Btx also showed complete loss of NMJ Nav1.4 channel clustering (Figure 4H). Importantly, the loss of NMJ Nav1.4 did not affect the total pool of Nav1.4 protein present in the muscle (Figure 4I), indicating that loss of muscle ankyrins did not globally affect Nav1.4 protein but rather prevented only the highly specific clustering of Nav1.4 at the NMJ. We also found that β1 spectrin is not clustered at the postsynaptic membranes of AnkR/B/G tcKO mice (Figure 4J), consistent with the observation that in neurons, spectrin localization and clustering is dictated by ankyrins [7, 19]. In contrast to

Nav1.4 and β1 spectrin, Ankyrin-binding dystrophin [18], which is also enriched in the postsynaptic junctional folds [20], is still clustered in AnkR/B/G tcKO mice (Figure 4K). Taken together, these results demonstrate that there is triple-redundancy among muscle ankyrins, and that they are required for the clustering of Nav1.4 at the NMJ.

Loss of NMJ Nav1.4 causes neuromuscular synapse fatigue

How does loss of Nav1.4 from the NMJ affect muscle function? Based on the proposed functions of postsynaptic NMJ Na^+ channels [4], we expected AnkR/B/G tcKO mice to be significantly impaired. However, simple visual inspection of tcKO mice showed they were indistinguishable from their floxed controls. Furthermore, we found that neither grip strength (Figure 5A) nor latency to fall from the rotarod (Figure 5B) was affected by loss of ankyrins, and this was true at both 2 and 5 months of age. To further determine if loss of muscle ankyrins impacts muscle function or health, we first measured extensor digitorum longus (EDL) muscle weight and found no difference between floxed control and AnkR/B/G tcKO mice (ctrl: 8.98 +/− 0.36 grams; tcKO: 9.35 +/− 0.23 grams, mean +/− SEM). We next measured the peak muscle force after direct muscle stimulation *ex vivo* and found no difference between floxed control and AnkR/B/G tcKO mice (Figure 5C). Finally, we measured the percent reduction in muscle force over 900s of direct muscle stimulation (Figure 5D); we found no significant difference between floxed control and tcKO mice. Histology of muscle cross sections also showed no indication of atrophy or muscle degeneration (Figure 5E). Together these results strongly suggest that loss of muscle ankyrins does not affect muscle strength or cause apparent muscle degeneration.

Mice will spontaneously run long distances and for long periods of time (4-6 hours) when a running wheel is included in their home cage. Therefore, to further examine muscle function in AnkR/B/G tcKO mice, we included freely accessible running wheels in their cages and measured their activity on the running wheel continuously for six days. We found that although tcKO and their floxed controls initially (day 1) spend the same amount of time on the running wheel and run for the same distance (Figures 5F and G), they rapidly diverge with tcKO mice spending significantly less time on the running wheel and running for significantly shorter distances for the remaining five days (Figures 5F and 5G). Since direct stimulation of muscles for a long period of time did not reveal any increased muscle fatigue in tcKO mice compared to controls (Figure 5D), our results suggest loss of ankyrins and NMJ Na1.4 channel clustering may cause neuromuscular synapses to fatigue with repeated use.

To further investigate NMJ function and more specifically the nerve-dependent muscle activation, we measured compound muscle action potentials (CMAPs) by stimulating the sciatic nerve and measuring CMAPs in the hind paw of all control, single, double, and triple conditional knockout mice; all mice had a normal appearing CMAP (data not shown). Since AnkR/B/G tcKO mice lack NMJ Na^+ channels, we next stimulated nerves at 20, 40, and 60 Hz. We found that after just a few stimulations, AnkR/B/G tcKO CMAP amplitudes rapidly declined and were significantly smaller than floxed controls at 40 and 60 Hz stimulation (Figure 5H). These results suggest that NMJ Nav1.4 prevents neuromuscular synapse fatigue in response to repetitive stimulation.

DISCUSSION

In this study we sought to answer two questions: 1) what molecular mechanisms underlie NMJ Nav1.4 channel clustering, and 2) what do clustered Na^+ channels do at the NMJ? To answer the first, we used nodes of Ranvier as a paradigm since the molecular mechanisms for nodal Na^+ channel clustering are worked out in detail [6]. Among nodal proteins only ankyrins are required for Na^+ channel clustering. Our experiments show that NMJ Nav1.4 clustering also requires ankyrins, that there is redundancy among the ankyrins, and the three vertebrate ankyrins have differing degrees of efficiency for channel clustering. Since the dcKO mice lacking AnkG had reduced NMJ Nav1.4 compared to dcKO mice with AnkG (Figure 3J), this suggests a hierarchy for channel clustering with AnkG being most efficient. These properties are similar to those found at nodes of Ranvier [7].

In contrast to the redundancy among ankyrins for NMJ Nav1.4 clustering, we found that NMJ KCNQ2-containing K^+ channels required AnkG and that neither AnkR nor AnkB can cluster KCNQ2. This observation matches that at nodes of Ranvier where in the absence of AnkG, nodal Na^+ channels but not nodal KCNQ2 K^+ channels are clustered by AnkR [21]. Interestingly, mutations in KCNQ2 cause episodic ataxia and myokymia (muscle rippling), but this is considered to be neuronal, rather than muscular, in origin [22] since these channels are also found at axon initial segments and nodes of Ranvier. KCNQ2 K^+ channels underlie IKs, a slow K^+ current which because of its slow kinetics is thought to exert very little influence on repolarization of the action potential [23]. Future studies of these K^+ channels will be required to define their roles at the NMJ.

While there are key similarities for Na^+ channel clustering between NMJ and nodes of Ranvier, there are also important differences. For example, nodal ankyrins, and their associated Na^+ channels, can be clustered through two distinct mechanisms: through binding to NF186 or by a paranodal spectrin-dependent cytoskeletal barrier. We did not detect NF186 at the NMJ, or any other L1CAM membrane protein (data not shown). One previous study reported that antibodies against phosphorylated-FIGQY, the common AnkG-binding motif in L1CAMs, label the vertebrate NMJ [24]. However, phosphorylation of the FIGQY motif inhibits ankyrin binding [25]. Alternatively, β-dystroglycan and dystrophin may function to recruit ankyrins to the NMJ, since both dystrophin and β-dystroglycan bind AnkG [18]. In support of this idea, we found that dystrophin was still appropriately clustered in the junctional folds of the endplate in the absence of muscle ankyrins, suggesting that its recruitment through β-dystroglycan may be dictated by extrinsic and ankyrin-independent mechanisms. Future studies will be required to determine if β-dystroglycan functions at the NMJ to recruit ankyrins, similar to how NF186 recruits ankyrins at nodes.

We found no evidence for enriched β4 spectrin at the vertebrate NMJ. This is surprising since at AIS and nodes of Ranvier, β4 spectrin is the obligate binding partner for AnkG [26, 27]. Furthermore, one previous study reported β4 spectrin at the sarcolemma and myopathy in a patient with loss of β4 spectrin [28]. Instead, among the β spectrins, we found only β1 spectrin at the NMJ; β1 spectrin is also found at nodes of Ranvier when AnkR is present [7, 29]. We found that NMJ ankyrins are required to cluster β1 spectrin. This is in contrast to previous studies at Drosophila NMJs where recruitment of postsynaptic

ankyrin was reported to depend on spectrins [30]. Furthermore, loss of post-synaptic spectrin in Drosophila disrupted subsynaptic muscle membranes, and active zone size and spacing. Future studies will be necessary to determine the function of β1 spectrin at the vertebrate NMJ, whether it binds to both AnkG and AnkR, and if, like at nodes of Ranvier, NMJ spectrins function mainly to stabilize and maintain ankyrin and Na^+ channel protein complexes [29].

Muscle AnkB was previously reported to be required for proper localization of dystrophin and adult NMJ morphology [18]. However, our results show that dystrophin and NMJ morphology are unaffected in muscle-specific ankyrin tcKO mice. Surprisingly, although we found that all three ankyrins can cluster NMJ Nav1.4, we were unable to detect AnkB enriched at the postsynaptic NMJ membrane like AnkR or AnkG. Instead, our results show that AnkB is more highly enriched in the presynaptic axon, and present at lower levels in the postsynaptic NMJ. If AnkB is not clustered at the NMJ, how does it function as a mechanism to cluster NMJ Nav1.4? It is possible that as for muscle AnkG, there are unique splice variants not detected using our antibodies. Alternatively, AnkB may not function in the junctional folds, but instead may participate in a cytoskeletal barrier surrounding the NMJ that functions like the cytoskeletal barrier at the distal end of the AIS or at the paranodal junctions flanking nodes of Ranvier [31, 32]. Since the dcKO mice lacking AnkG/AnkR have reduced amounts of NMJ Nav1.4 channels, such a cytoskeletal barrier mechanism is less efficient than when Nav1.4 binds directly to AnkG.

Our results, combined with previous studies of ankyrins in neurons, show surprising degrees of ankyrin redundancy that depend on subcellular context. For example, all three vertebrate ankyrins can cluster NMJ Nav1.4, but only AnkG can cluster AIS Na^+ channels, despite the expression of all three ankyrins in vertebrate neurons. Although greater redundancy is usually thought to imply more essential functions, loss of all muscle ankyrins is not lethal and phenotypes are mild. In contrast, loss of AIS AnkG alone causes death at birth [7, 17], and simultaneous loss of AnkR and AnkG from sensory neurons causes death within one week of birth [7]. Paradoxically, the greater the redundancy for ankyrins in Na^+ channel clustering, the less important the Na^+ channel clustering actually is for survival.

What do clustered Na^+ channels do at the NMJ? In our experiments we showed that ankyrin-deficient muscles had normal amounts of total Nav1.4, but no clustered NMJ Nav1.4. Thus, an ankyrin-dependent NMJ Nav1.4 channel clustering mechanism provides a unique opportunity to test the specific function of NMJ Na^+ channels. Behaviorally, we found that cKO, dcKO, and tcKO mice were indistinguishable from their controls on the rotarod. Furthermore, AnkR/B/G tcKO mice had normal grip strength, peak muscle force, and percent muscle force over time. These results were surprising since NMJ Na^+ channels were previously thought to be important for efficient synaptic transmission and muscle function [4, 9]. Nevertheless, we found that AnkR/B/G tcKO mice were significantly less active and ran for significantly shorter distances on a running wheel than their floxed controls. Most importantly, direct and repeated nerve stimulation followed by measurement of CMAPs showed that tcKO neuromuscular synapses fatigue significantly more quickly than control mice. Synaptic transmission failure can result from several postsynaptic mechanisms including AchR desensitization and reduced sarcolemmal excitability. Our experiments

suggest that ankyrin-dependent clustering of NMJ Nav1.4 Na^+ channels in the junctional folds increases the safety factor to prevent neuromuscular synapse fatigue and synaptic transmission failure. We speculate that during aging, clustered NMJ Nav1.4 may protect against fatigue, while during injury loss of clustered NMJ Nav1.4 may contribute to muscle fatigue.

STAR METHODS

RESOURCE AVAILABILITY

Lead Contact—Further information and requests for resources and reagents should be directed to and will be fulfilled by the Lead Contact, Dr. Matthew Rasband (rasband@bcm.edu).

Materials Availability—This study did not generate new unique reagents.

Data and Code availability

- All data reported in this paper will be shared by the lead contact upon request.
- This paper does not report original code.
- Any additional information required to reanalyze the data reported in this paper is available from the lead contact upon request.

EXPERIMENTAL MODEL AND SUBJECT DETAILS

Mouse lines—*Myo-Cre* were kindly provided by Dr. Eric Olson (Department of Molecular Biology, UT Southwestern Medical Center). *Ank1*$^{f/f}$, *Ank2*$^{f/f}$, or *Ank3*$^{f/f}$ mice were all described previously [7, 33, 34]. Animals were housed with a 12/12 h light/dark cycle and free access to food and water. Both male and female mice were used in our experiments. All experiments were approved by the Institutional Animal Care and Use Committee (IACUC) of Baylor College of Medicine and were performed in accordance with the National Institutes of Health guidelines for the care and use of laboratory animals.

METHOD DETAILS

Immunofluorescence labeling and microscopy—For NMJ staining, whole-mount hind-limb lumbrical muscles were stained as previously described [35]. Briefly, the hind-limbs of the mouse are isolated and foot skin detached. The flexor digitorum brevis (FDB) tendon is cut transversely near the ankle, lifted up and the entire muscle mass is isolated by cutting the distal ends of the tendon. The FDB tendon is placed with ventral side up, the lumbrical muscles are located between the tendon ends and can be collected by removing the connective tissues. Dissected lumbrical muscles were fixed in 4% paraformaldehyde (PFA) in 0.1 m phosphate buffer (PB) at 4°C for 15 min, rinsed three times with PBS (pH 7.4). Muscles were permeabilized in 24 well plates with 2% (v/v) Triton X-100 in PBS for 30 min. They were blocked in 10% (v/v) normal goat serum and 1% (v/v) Triton X-100 in PBS for 30 min. Samples were incubated overnight at 4 °C in blocking solution with primary antibodies. After washing four times for 20 min each with 1% Triton X-100 in PBS, tissues were incubated with Alexa Fluor 350-conjugated or Alexa Fluor 594-conjugated

secondary antibody and Alexa Fluor 488-conjugated α-BTX for 2 h at room temperature. After washing four times for 20 min each with 1% Triton X-100 in PBS, tissues were mounted in mounting medium and covered with a coverslip. Z-serial images were collected with a Nikon fluorescence microscope (Nikon Eclipse Ni-E microscope) and projected into a single image. The fluorescence intensity was quantified using NIH FIJI/ImageJ software. In brief, each NMJ was manually traced, after which area, mean fluorescence were measured. The background fluorescence was also measured. The corrected total fluorescence intensity was calculated after background subtraction. For all measurements of Nav1.4/Btx ratios experimenters were blinded to genotype.

Muscle Histology—EDL muscles were dissected then immediately frozen in OCT using liquid nitrogen. Muscles were cryosectioned at 25 μm, collected on microscope slides and stored at −80 until staining. For staining, room temperature slides with mounted sections were immersed for 10 minutes in hematoxylin staining solution. Slides were rinsed repeatedly, then immersed in Eosin solution for three minutes, then again rinsed repeatedly. Stained slides were then successively immersed and transferred from 50% ethanol for 20 sec, 70% ethanol for 20 sec, 90% ethanol for 20 sec, 100% ethanol for 1 min and xylene for 3 min. The labeled sections were then dried and mounted with coverslips.

SDS-PAGE and Immunoblot Analysis—Immunoblot analysis was performed using tibialis anterior muscles. Samples were homogenized in 50mM Tris-HCL, (pH7.6), 15mM NaCl, 2mM EDTA, 1 % NP-40, 10mM PMSF, and 10 μg/mL aprotinin. Total protein levels were measured using the bicinchoninic acid assay (BCA); proteins (50 μg/sample) were size fractionated on SDS-PAGE gels and subsequently transferred to nitrocellulose blotting membrane (GE Healthcare Life sciences) using a Trans-Blot Turbo Transfer System (Bio-Rad, Hercules, CA). Nitrocellulose membranes were blocked for 1hour at room temperature in 5% bovine serum albumin (BSA). Membranes were then probed with primary antibodies and secondary antibodies. After extensive washing, the membranes were incubated with SuperSignal West Pico Plus Chemiluminescent Substrate (Thermo Scientific).

Behavioral Assays—An accelerating rod (Ugo Basile) was used to measure the motor coordination and balance of the animals. In brief, mice were placed on a rotating rod (3-cm diameter) and the time each animal was able to stay on the rod was recorded. The rotarod's speed increased from 4 to 40 rpm over a 5-min period. Mice were pre-trained for one trial on the accelerating rod before the test. A grip-strength meter (Columbus Instruments) was used to measure the general neuromuscular strength. Mice were held and lowered toward the meter, allowed to grasp a metal rod, and then pulled horizontally away from the rod. The force on the bar when the grasp was released was recorded as the grip strength. Spontaneous wheel running was assessed using the Respironics MiniMitter Vitalview system with stainless steel running wheels (diameter: 11cm, width 5cm) in Tecniplast housing cages (30cm x 15cm). Animals were maintained on a 12:12 light/dark cycle with the light phase from 6:00am – 6:00pm. Distance traveled by wheel running was quantified using the Vitalview software based on the wheel revolutions detected via magnetic reed switch sensors. Animals were recorded for 6 days, and provided *ad libitum* with access to food and water. Animals and wheel running instruments were monitored daily

to confirm the health of the animals and the functioning of the sensors. For all behavioral experiments, experimenters were blinded to study groups.

NMJ Morphology Analysis—The post synaptic morphology of control and ankyrin triple knock out NMJs was analyzed using an NMJ Morph protocol [36]. Briefly, using Fiji [37], fluorescent micrographs of the post synaptic apparatus labelled with αBtx were manually thresholded to create a binary image. A polygonal region of interest was drawn around the binary image. The area of the thresholded pixels and the area of the region of interest was measured corresponding to AChR area and endplate area respectively. The AChR area was divided by the endplate area to record the compactness of the NMJ. Fragments were counted by using the analyze particles tool on the thresholded image. Non-continuous receptor clusters that were larger than 5 μm^2 were included in the counts for each NMJ. 47 – 50 NMJs per condition were measured.

Measurement of CMAPs—CMAPs were measured using a PowerLab signal acquisition system (AD Instruments, CO, USA) as described [38] with modifications. Briefly, mice were anesthetized with isoflurane/oxygen inhalation with a controlled body temperature of 37° C. The sciatic nerve was stimulated by inserting stimulating electrodes at the sciatic notch and the signal was recorded at the foot by inserting recording electrodes in the hindpaw. For single CMAP measurement, the nerve was stimulated with single pulse of 0.2 ms duration, with supramaximal current ranging up to 10 mA at 1 Hz. Signals were recorded at 40 kHz. To investigate synapse fatigue, the baseline CMAP was measured before stimulating the nerve with pulses of 0.2 ms duration repeated at 20, 40, or 60 Hz for a total of one second. Another baseline CMAP was recorded 30 seconds after high frequency stimulation. CMAP amplitude was defined by the difference in mV between depolarization and repolarization voltage. The recordings were analyzed using LabChart version 8 (AD Instruments, CO, USA).

Muscle Force Analysis—The extensor digitorum longus (EDL) muscle was surgically dissected. One end of the EDL was attached to a fixed hook and the other to a force transducer (F30, Harvard Apparatus) using silk suture (5-0). The muscle was placed in a physiological saline solution containing (in mM): 2.0 $CaCl_2$, 120.0 NaCl, 4.0 KCl, 1.0 $MgSO_4$, 25.0 $NaHCO_3$, 1.0 KH_2PO_4, 10.0 glucose, 0.0005 d-tubocurare, pH 7.3 and continuously gassed with 95% O_2–5% CO_2 at 25 °C. Optimal muscle length (L_o) and voltage (V_{max}) were adjusted to elicit maximum twitch force. Force was measured in response to 60Hz stimulation (pulse and train durations of 0.5 and 250 ms, respectively) every 30s for 900s At the end of the contractile protocol muscle length was measured using a hand-held electronic caliper and fiber bundles were trimmed of excess connective tissue, blotted dry, and weighed.

QUANTIFICATION AND STATISTICAL ANALYSIS

All statistical analyses were performed using GraphPad Prism. Statistical tests used for comparisons are indicated in each figure legend. All statistical comparisons are shown with error bars +/− SEM.

ACKNOWLEDGMENTS

The work reported here was supported by the following research grants: NIH AR074988 and by the Dr. Miriam and Sheldon G. Adelson Medical Research Foundation.

REFERENCES

1. Sanes JR, and Lichtman JW (2001). Induction, assembly, maturation and maintenance of a postsynaptic apparatus. Nat Rev Neurosci 2, 791–805. [PubMed: 11715056]
2. Beam KG, Caldwell JH, and Campbell DT (1985). Na channels in skeletal muscle concentrated near the neuromuscular junction. Nature 313, 588–590. [PubMed: 2578630]
3. Caldwell JH (2000). Clustering of sodium channels at the neuromuscular junction. Microsc Res Tech 49, 84–89. [PubMed: 10757881]
4. Slater CR (2008). Structural factors influencing the efficacy of neuromuscular transmission. Ann N y Acad Sci 1132, 1–12. [PubMed: 18096848]
5. Mahmud M, Rahman MM, and Vassanelli S (2012). Na+ channels at postsynaptic muscle membrane affects synaptic transmission at neuromuscular junction: a simulation study. Annu Int Conf IEEE Eng Med Biol Soc 2012, 3616–3619.
6. Rasband MN, and Peles E (2021). Mechanisms of node of Ranvier assembly. Nat Rev Neurosci 22, 7–20. [PubMed: 33239761]
7. Ho TS, Zollinger DR, Chang KJ, Xu M, Cooper EC, Stankewich MC, Bennett V, and Rasband MN (2014). A hierarchy of ankyrin-spectrin complexes clusters sodium channels at nodes of Ranvier. Nat Neurosci 17, 1664–1672. [PubMed: 25362473]
8. Kordeli E, Ludosky MA, Deprette C, Frappier T, and Cartaud J (1998). AnkyrinG is associated with the postsynaptic membrane and the sarcoplasmic reticulum in the skeletal muscle fiber. J Cell Sci 111 (Pt 15), 2197–2207. [PubMed: 9664041]
9. Bailey SJ, Stocksley MA, Buckel A, Young C, and Slater CR (2003). Voltage-gated sodium channels and ankyrinG occupy a different postsynaptic domain from acetylcholine receptors from an early stage of neuromuscular junction maturation in rats. J Neurosci 23, 2102–2111. [PubMed: 12657669]
10. Wood SJ, and Slater CR (1998). beta-Spectrin is colocalized with both voltage-gated sodium channels and ankyrinG at the adult rat neuromuscular junction. J Cell Biol 140, 675–684. [PubMed: 9456326]
11. Eshed-Eisenbach Y, and Peles E (2019). The clustering of voltage-gated sodium channels in various excitable membranes. Dev Neurobiol.
12. Garrido JJ, Giraud P, Carlier E, Fernandes F, Moussif A, Fache MP, Debanne D, and Dargent B (2003). A targeting motif involved in sodium channel clustering at the axonal initial segment. Science 300, 2091–2094. [PubMed: 12829783]
13. Gasser A, Ho TS-Y, Cheng X, Chang KJ, Waxman SG, Rasband MN, and Dib-Hajj S (2012). An ankyrinG-binding motif is necessary and sufficient for targeting Nav1.6 Na+ channels to axon initial segments and nodes of Ranvier. J Neurosci 32, 7232–7243. [PubMed: 22623668]
14. Jenkins PM, Kim N, Jones SL, Tseng WC, Svitkina TM, Yin HH, and Bennett V (2015). Giant ankyrin-G: a critical innovation in vertebrate evolution of fast and integrated neuronal signaling. Proc Natl Acad Sci U S A 112, 957–964. [PubMed: 25552556]
15. Pan Z, Kao T, Horvath Z, Lemos J, Sul J-Y, Cranstoun SD, Bennett MV, Scherer SS, and Cooper EC (2006). A common ankyrin-G-based mechanism retains KCNQ and Nav channels at electrically active domains of the axon. J Neurosci 26, 2599–2613. [PubMed: 16525039]
16. Hill AS, Nishino A, Nakajo K, Zhang G, Fineman JR, Selzer ME, Okamura Y, and Cooper EC (2008). Ion channel clustering at the axon initial segment and node of ranvier evolved sequentially in early chordates. PLoS Genet 4, e1000317. [PubMed: 19112491]
17. Liu CH, Seo R, Ho TS, Stankewich M, Mohler PJ, Hund TJ, Noebels JL, and Rasband MN (2020). beta spectrin-dependent and domain specific mechanisms for Na(+) channel clustering. eLife 9.

18. Ayalon G, Davis JQ, Scotland PB, and Bennett V (2008). An ankyrin-based mechanism for functional organization of dystrophin and dystroglycan. Cell 135, 1189–1200. [PubMed: 19109891]
19. Yang Y, Ogawa Y, Hedstrom KL, and Rasband MN (2007). βIV spectrin is recruited to axon initial segments and nodes of Ranvier by ankyrinG. J Cell Biol 176, 509–519. [PubMed: 17283186]
20. Khurana TS, Watkins SC, Chafey P, Chelly J, Tome FM, Fardeau M, Kaplan JC, and Kunkel LM (1991). Immunolocalization and developmental expression of dystrophin related protein in skeletal muscle. Neuromuscul Disord 1, 185–194. [PubMed: 1822793]
21. Wang CC, Ortiz-Gonzalez XR, Yum SW, Gill SM, White A, Kelter E, Seaver LH, Lee S, Wiley G, Gaffney PM, et al. (2018). betaIV Spectrinopathies Cause Profound Intellectual Disability, Congenital Hypotonia, and Motor Axonal Neuropathy. Am J Hum Genet 102, 1158–1168. [PubMed: 29861105]
22. Dedek K, Kunath B, Kananura C, Reuner U, Jentsch TJ, and Steinlein OK (2001). Myokymia and neonatal epilepsy caused by a mutation in the voltage sensor of the KCNQ2 K+ channel. Proc Natl Acad Sci U S A 98, 12272–12277. [PubMed: 11572947]
23. Schwarz JR, Glassmeier G, Cooper EC, Kao TC, Nodera H, Tabuena D, Kaji R, and Bostock H (2006). KCNQ channels mediate IKs, a slow K+ current regulating excitability in the rat node of Ranvier. J Physiol 573, 17–34. [PubMed: 16527853]
24. Jenkins SM, Kizhatil K, Kramarcy NR, Sen A, Sealock R, and Bennett V (2001). FIGQY phosphorylation defines discrete populations of L1 cell adhesion molecules at sites of cell-cell contact and in migrating neurons. J Cell Sci 114, 3823–3835. [PubMed: 11719549]
25. Garver TD, Ren Q, Tuvia S, and Bennett V (1997). Tyrosine phosphorylation at a site highly conserved in the L1 family of cell adhesion molecules abolishes ankyrin binding and increases lateral mobility of neurofascin. J Cell Biol 137, 703–714. [PubMed: 9151675]
26. Berghs S, Aggujaro D, Dirkx R, Maksimova E, Stabach P, Hermel JM, Zhang JP, Philbrick W, Slepnev V, Ort T, et al. (2000). betaIV spectrin, a new spectrin localized at axon initial segments and nodes of ranvier in the central and peripheral nervous system. J Cell Biol 151, 985–1002. [PubMed: 11086001]
27. Komada M, and Soriano P (2002). βIV-spectrin regulates sodium channel clustering through ankyrin-G at axon initial segments and nodes of Ranvier. J Cell Biol 156, 337–348. [PubMed: 11807096]
28. Knierim E, Gill E, Seifert F, Morales-Gonzalez S, Unudurthi SD, Hund TJ, Stenzel W, and Schuelke M (2017). A recessive mutation in beta-IV-spectrin (SPTBN4) associates with congenital myopathy, neuropathy, and central deafness. Hum Genet 136, 903–910. [PubMed: 28540413]
29. Liu CH, Stevens SR, Teliska LH, Stankewich M, Mohler PJ, Hund TJ, and Rasband MN (2020). Nodal beta spectrins are required to maintain Na(+) channel clustering and axon integrity. eLife 9.
30. Pielage J, Fetter RD, and Davis GW (2006). A postsynaptic spectrin scaffold defines active zone size, spacing, and efficacy at the Drosophila neuromuscular junction. J Cell Biol 175, 491–503. [PubMed: 17088429]
31. Zhang C, Susuki K, Zollinger DR, Dupree JL, and Rasband MN (2013). Membrane domain organization of myelinated axons requires betaII spectrin. J Cell Biol 203, 437–443. [PubMed: 24217619]
32. Galiano MR, Jha S, Ho TS, Zhang C, Ogawa Y, Chang KJ, Stankewich MC, Mohler PJ, and Rasband MN (2012). A distal axonal cytoskeleton forms an intra-axonal boundary that controls axon initial segment assembly. Cell 149, 1125–1139. [PubMed: 22632975]
33. Chang KJ, Zollinger DR, Susuki K, Sherman DL, Makara MA, Brophy PJ, Cooper EC, Bennett V, Mohler PJ, and Rasband MN (2014). Glial ankyrins facilitate paranodal axoglial junction assembly. Nat Neurosci 17, 1673–1681. [PubMed: 25362471]
34. Stevens SR, et al. (2021). Ankyrin-R regulates fast-spiking interneuron excitability through perineuronal nets and Kv3.1b K+ channels. in review.
35. Sleigh JN, Burgess RW, Gillingwater TH, and Cader MZ (2014). Morphological analysis of neuromuscular junction development and degeneration in rodent lumbrical muscles. J Neurosci Methods 227, 159–165. [PubMed: 24530702]

36. Jones RA, Reich CD, Dissanayake KN, Kristmundsdottir F, Findlater GS, Ribchester RR, Simmen MW, and Gillingwater TH (2016). NMJ-morph reveals principal components of synaptic morphology influencing structure-function relationships at the neuromuscular junction. Open Biol 6.

37. Schindelin J, Arganda-Carreras I, Frise E, Kaynig V, Longair M, Pietzsch T, Preibisch S, Rueden C, Saalfeld S, Schmid B, et al. (2012). Fiji: an open-source platform for biological-image analysis. Nature methods 9, 676–682. [PubMed: 22743772]

38. Pollari E, Prior R, Robberecht W, Van Damme P, and Van Den Bosch L (2018). In Vivo Electrophysiological Measurement of Compound Muscle Action Potential from the Forelimbs in Mouse Models of Motor Neuron Degeneration. J Vis Exp.

Highlights:

- Ankyrin scaffolding proteins cluster Nav1.4 channels at neuromuscular junctions
- Ankyrin-deficient muscles have normal muscle force and do not degenerate
- Nav1.4 channel clustering prevents neuromuscular synapse fatigue

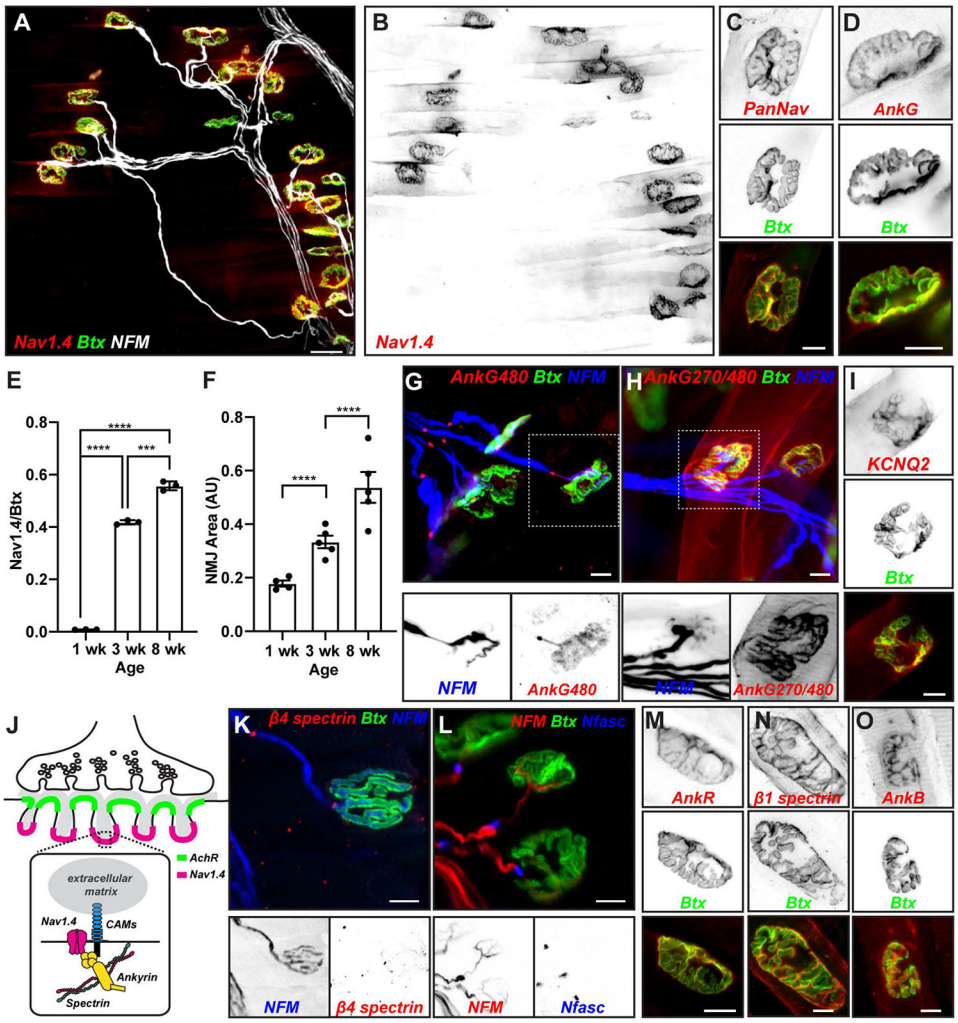

Figure 1. The neuromuscular junction is highly enriched in Nav1.4 Na^+ channels, ankyrins and spectrins.

(A) Labeling of adult mouse lumbrical muscles using fluorescent α-bungarotoxin (Btx, green), and antibodies against Nav1.4 (red) and neurofilament-M (NFM, white). Scale bar = 30 μm. (B) Nav1.4 immunostaining of muscle shown in (A). (C, D) Immunostaining of NMJ using PanNav (C) and AnkG (D) antibodies (red) and Btx (green). Scale bars = 10 μm. (E) The ratio of Nav1.4 fluorescence to Btx fluorescence at NMJs at 1, 3, and 8 weeks of age. N= 3 mice/age, n=20 NMJs/mouse. ***, p<0.001; ****, p<0.0001; Students's t-test. Error bars, +/− SEM. (F) Relative increase in NMJ area during development. AU, arbitrary units. N= 4-5 mice. n= 38-44 NMJs. ****, p<0.0001; Students's t-test. Error bars, +/− SEM. (G, H) Immunostaining of lumbrical muscle using antibodies against AnkG480 (G, red) or AnkG270/480 (H, red), NFM (blue), and Btx (green). Boxed regions showing NFM and AnkG labeling is shown in lower panels. Scale bars = 10 μm. (I) Immunostaining of NMJ for KCNQ2 K^+ channels and Btx. Scale bar = 10 μm. (J) Cartoon of NMJ showing the proposed molecular interactions responsible for Nav1.4 clustering in the junctional folds. (K) Immunostaining of lumbrical muscle using antibodies against β4 spectrin (red), NFM (blue), and Btx (green). Boxed regions showing NFM and β4 spectrin labeling is

shown in lower panels. Scale bars = 10 μm. (L) Immunostaining of lumbrical muscle using antibodies against neurofascin (Nfasc) (blue), NFM (red), and Btx (green). Boxed regions showing NFM and Nfasc labeling is shown in lower panels. Scale bars = 10 μm. (M-O) Immunostaining of NMJs using antibodies against AnkR (M), β1 spectrin (N), and AnkB (O), and Btx (green). Scale bars = 10 μm.

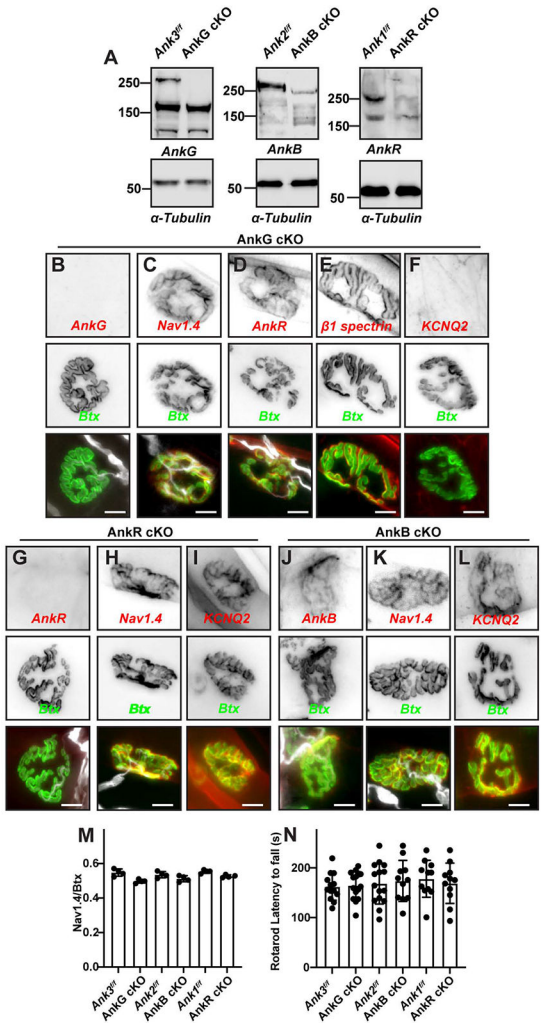

Figure 2. Loss of a single muscle ankyrin does not impair Nav1.4 channel clustering or muscle function.

(A) Immunoblots of AnkG cKO, AnkB cKO, and AnkR cKO and their floxed controls. (B-F) Labeling of AnkG cKO NMJs using antibodies against AnkG (B), Nav1.4 (C), AnkR (D), β1 spectrin (E), KCNQ2 (F), NFM (white, except for panels (E and F)), and Btx (green). Scale bars = 10 μm. (G-L) Immunostaining of AnkR cKO (G-I) and AnkB cKO (J-L) mice for AnkR (G), AnkB (J), Nav1.4 (H, K), and KCNQ2 (I, L), NFM (white), and Btx (green). Scale bars = 10 μm. (M) The ratio of Nav1.4 fluorescence to Btx fluorescence at NMJs in AnkG, AnkB, and AnkR cKO mice compared to their floxed controls. N= 4 mice, n=26 NMJs/mouse; all mice were 2 months old. Error bars, +/− SEM. (N) Latency to fall in seconds from the rotarod for 2 month-old mice of the indicated genotypes. N=11-15 mice per genotype. Error bars, +/− SEM. Statistical comparisons were performed using the Mann-Whitney test.

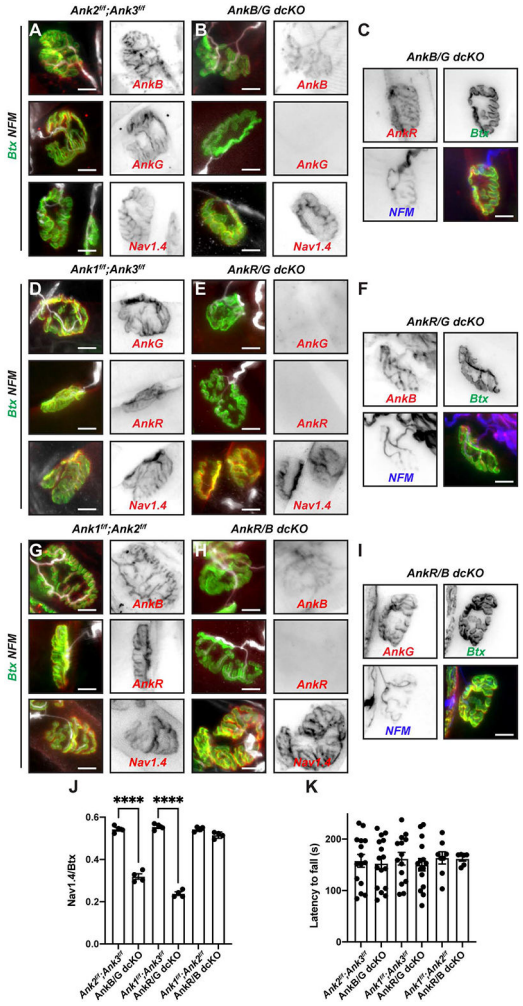

Figure 3. Loss of two muscle ankyrins.

(A-C) Immunostaining of control (A) and AnkB/G dcKO (B, C) NMJs using the indicated antibodies and Btx. (D-F) Immunostaining of control (D) and AnkR/G dcKO (E, F) NMJs using the indicated antibodies and Btx. (G-I) Immunostaining of control (G) and AnkR/B dcKO (H, I) NMJs using the indicated antibodies and Btx. For A-I, scale bars = 10 μm. (J) The ratio of Nav1.4 fluorescence to Btx fluorescence at NMJs in dcKO mice compared to their floxed controls. N= 4 mice/age, n=22-26 NMJs/mouse; all mice were 2 months old. ****, $p<0.0001$; Student's t-test with Welch's correction. Error bars, +/− SEM. (K) Latency to fall in seconds from the rotarod for 2 month-old mice of the indicated genotypes. N=6-16 mice per genotype. Statistical comparison showed no significant difference using the Mann-Whitney test. Error bars, +/− SEM.

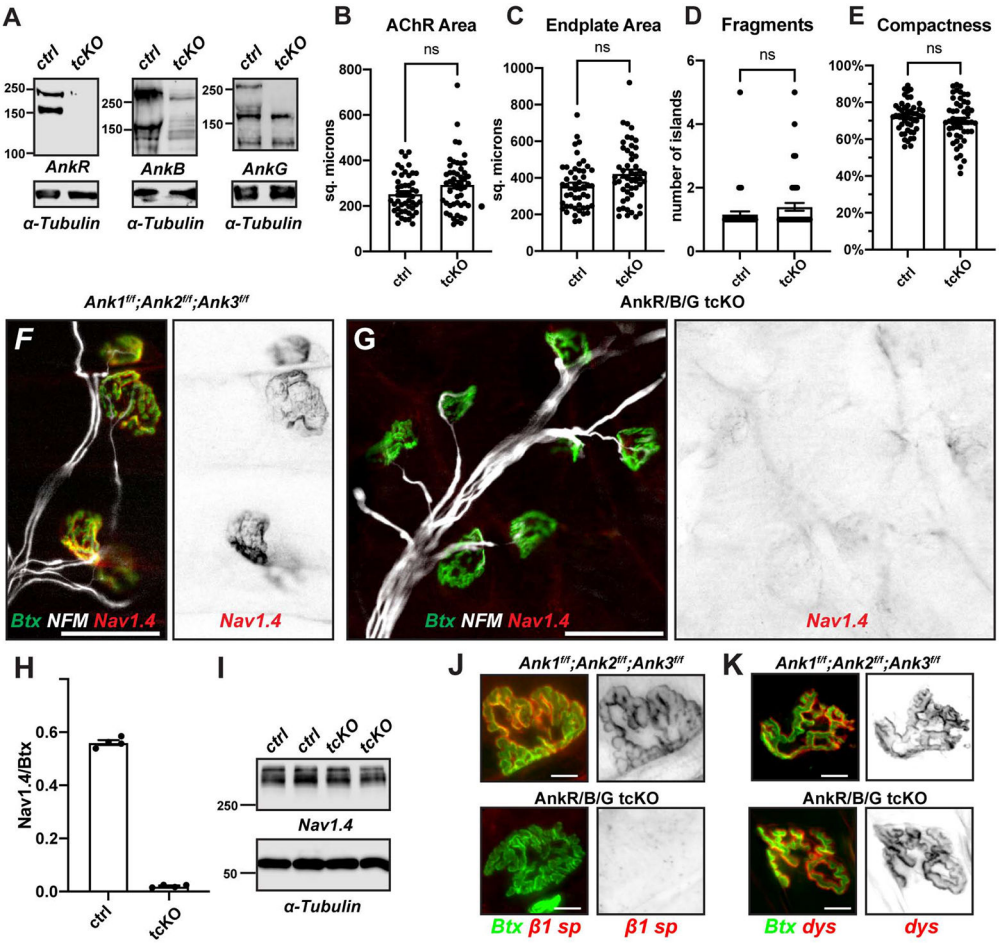

Figure 4. Muscle-specific triple ankyrin knockouts lack clustered NMJ Nav1.4.

(A) Immunoblots of tcKO muscles using antibodies against AnkR, AnkB, and AnkG, and α-Tubulin as a loading control. (B-E) Morphometric analysis of NMJs. (F, G) Immunostaining of control (F) and tcKO (G) mice for Nav1.4 (red and inverted image at right) and NFM (white), and labeling of NMJs using Btx (green). Scale bars = 50 μm. (H) The ratio of Nav1.4 fluorescence to Btx fluorescence at NMJs in tcKO mice compared to their floxed controls. N= 4 mice/age, n=22-26 NMJs/mouse; all mice were 2 months old. (I) Immunoblot showing the amount of Nav1.4 protein in control and tcKO mice with α-Tubulin as a loading control. (J, K) Labeling of control and tcKO NMJ for β1 spectrin (J, red) or dystrophin (K, red) and Btx (green). Scale bars = 10 μm. All statistical comparisons were performed using Student's t-test with Welch's correction. Error bars, +/− SEM.

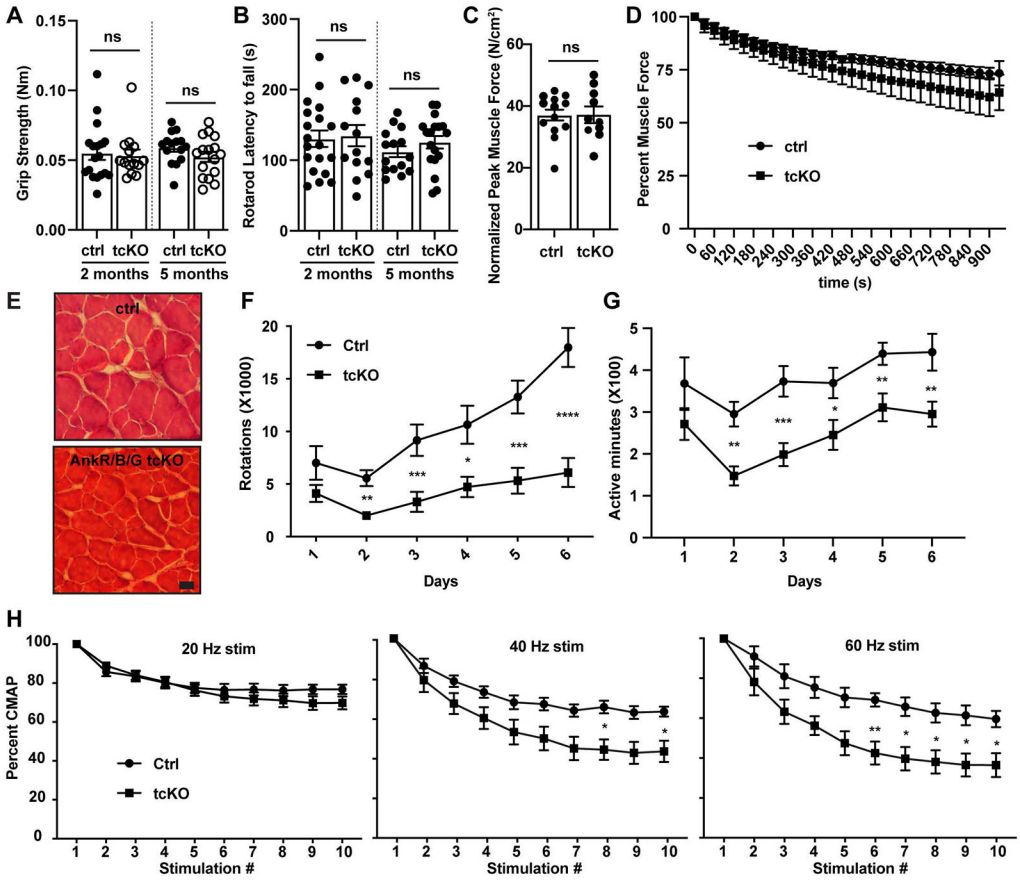

Figure 5. Loss of NMJ Nav1.4 results in neuromuscular synapse fatigue.

(A) Comparison of grip strength between control and tcKO mice at 2 and 5 months of age. N=14-18 mice per genotype. ns, not significant Student's t-test. (B) Comparison of latency to fall from the rotarod between control and tcKO mice at 2 and 5 months of age. N= 14-19 mice per genotype. ns, not significant Student's t-test. (C) Normalized peak muscle force in N/cm^2. N= 13 control, 10 tcKO mice. (D) Comparison of muscle force measured ex vivo between control and tcKO mice. N=13 control, 10 tcKO mice. Differences were not significant as determined using the multiple Kolmogorov-Smirnov test. (E) Hematoxylin and eosin staining of control and tcKO muscles cross sections. Scale bar = 36 μm. (F, G) Average number of rotations (F) and active minutes (G) by control and tcKO mice on a running wheel for 6 days. N=11 control, 13 tcKO mice. *, p<0.01; **, p<0.001; ***, p<0.0001; ****, p<0.00001; statistical comparison was performed using the Mann-Whitney test. (H) Measurement of compound muscle action potential (CMAP) as a percentage of the first CMAP during 20, 40, or 60 kHz stimulation. N= 11 control, 13 tckO mice *, p<0.01, **, p<0.001; statistical comparison was determined using the multiple Kolmogorov-Smirnov test. All error bars +/− SEM.

KEY RESOURCES TABLE

REAGENT or RESOURCE	SOURCE	IDENTIFIER
Antibodies		
mouse monoclonal anti-Nav1.4 clone N255/38	Neuromab	RRID:AB_2877201
mouse monoclonal anti-Pan Nav sodium channel clone N419/78	Neuromab	RRID:AB_2877588
mouse monoclonal anti-AnkG clone 106/36	Neuromab	RRID:AB_2877524
mouse monoclonal anti-β1 Spectrin clone N385/21	Neuromab	RRID:AB_2877418
goat polyclonal anti-AnkG	Dr. Vann Bennett, Duke University	N/A
rabbit polyclonal anti-AnkB	Rasband lab	RRID:AB_2315635
rabbit polyclonal anti-AnkR	Rasband lab	RRID:AB_2833096
Mouse monoclonal anti-α-Tubulin	Sigma	RRID:AB_477582
rabbit polyclonal anti-dystrophin	Abcam	RRID: AB_301813
rabbit polyclonal anti-β4 spectrin	Rasband lab	RRID: AB_2315634
mouse monoclonal Neurofilament-M clone 2H3	Developmental Studies Hybridoma Bank	RRID:AB_531793
Rabbit polyclonal anti-AnkG480	Dr. Paul Jenkins, University of Michigan	N/A
Rabbit polyclonal anti-AnkG270/480	Dr. Paul Jenkins, University of Michigan	N/A
Chicken anti-Neurofascin	R&D Systems	RRID:AB_10890736
Alexa Fluor 594 goat anti-rabbit IgG	Thermofisher	RRID:AB_2534079
Alexa Fluor 594 goat anti-mouse IgG1	Thermofisher	RRID:AB_2535767
Alexa Fluor 594 goat anti-mouse IgG2a	Thermofisher	RRID:AB_2535774
Alexa Fluor 594 goat anti-mouse IgG2b	Thermofisher	RRID:AB_2535781
Alexa Fluor 350 goat anti-mouse IgG	Thermofisher	RRID:AB_2534100
horseradish peroxidase (HRP)-conjugated goat anti-rabbit IgG	Jackson ImmunoResearch	Cat # 111-035-003
horseradish peroxidase (HRP)-conjugated goat anti-mouse IgG	Jackson ImmunoResearch	Cat # 115-035-146
Chemicals, peptides, and recombinant proteins		
Alexa Fluor 488 α-Bungarotoxin	Thermofisher	Cat # B13422
Eosin Y sodium salt	Santa Cruz Biotechnology	Cat# sc-203734
Hematoxylin Solution	Ricca Chemical Company	Cat# 3530-16
d-tubocurare	Sigma	Cat# 5.05145
Supersignal West Pico plus chemiluminescent substrate	Thermofisher	Cat# 34579
Triton X-100	Sigma	Cat# X100
Paraformaldehyde	Sigma	Cat# 441244
Goat Serum	Sigma	Cat# G9023
Tissue plus OCT compound	Fisher Scientific	Cat# 23-730-571
Experimental models: Organisms/strains		
Myo-cre	Dr. Eric Olson, UT Southwestern	N/A

REAGENT or RESOURCE	SOURCE	IDENTIFIER
Ank1$^{f/f}$	Rasband lab	JAX mice, stock number 036512
Ank2$^{f/f}$	Peter Mohler, Ohio State University	JAX mice, stock number 031428
Ank3$^{f/f}$	Vann Bennett, Duke University	JAX mice, stock number 029797
Oligonucleotides		
Genotyping primers for *Myo-cre:* AGGTTCGTTCACTCATGGA TCGACCAGTTTAGTTACCC	This paper	N/A
Genotyping primers for *Ank1*$^{f/f}$*:* GGGAAACTCCACAGAGCCTGACGGGTCAGT GGCGTCCCTATGTTCCATCCTATAGATGACT	This paper	N/A
Genotyping primers for *Ank2*$^{f/f}$*:* GCAGTCTCAACACAACTAAGCCATCCTTTA GCTGAGGAGGTAGACAAGAACCTTTTTGTG	This paper	N/A
Genotyping primers for *Ank3*$^{f/f}$*:* TTGGGATGCTTTGATTCAGGG TTAATTTGGGGAGGGGGGAGTC	This paper	N/A
Software and algorithms		
Fiji	[37]	https://imagej.net/Fiji/Downloads
Prism	Graphpad	RRID:SCR_002798
Labchart version 8	AD Instruments	RRID:SCR_017551